Published online 19 October 2016 *Nucleic Acids Research, 2016, Vol. 44, No. 21* **10505–10514**
doi: 10.1093/nar/gkw941

Molecular mechanism of divalent-metal-induced activation of NS3 helicase and insights into Zika virus inhibitor design

Xiaocong Cao[1,†], Yajuan Li[1,*,†], Xiangyu Jin[1], Yuelong Li[1], Feng Guo[2] and Tengchuan Jin[1,*]

[1]Laboratory of Structural Immunology, CAS Key Laboratory of Innate Immunity and Chronic Disease, CAS Center for Excellence in Molecular Cell Science, School of Life Sciences and Medical Center, University of Science and Technology of China, Hefei, Anhui 230027, China and [2]School of Medicine, Stanford University, Stanford, CA 94305, USA

Received August 19, 2016; Revised October 03, 2016; Editorial Decision October 04, 2016; Accepted October 18, 2016

ABSTRACT

Zika virus has attracted increasing attention because of its potential for causing human neural disorders, including microcephaly in infants and Guillain–Barré syndrome. Its NS3 helicase domain plays critical roles in NTP-dependent RNA unwinding and translocation during viral replication. Our structural analysis revealed a pre-activation state of NS3 helicase in complex with GTPγS, in which the triphosphate adopts a compact conformation in the absence of any divalent metal ions. In contrast, in the presence of a divalent cation, GTPγS adopts an extended conformation, and the Walker A motif undergoes substantial conformational changes. Both features contribute to more extensive interactions between the GTPγS and the enzyme. Thus, this study provides structural evidence on the allosteric modulation of $MgNTP^{2-}$ on the NS3 helicase activity. Furthermore, the compact conformation of inhibitory NTP identified in this study provides precise information for the rational drug design of small molecule inhibitors for the treatment of ZIKV infection.

INTRODUCTION

Zika virus (ZIKV), a member of the *flaviviridae* family, is mainly spread by *Aedes* mosquitoes (1). Although most cases of ZIKV infection produce no symptoms, this virus may be associated with various severe neural disorders, including a brain defect in newborn called microcephaly (2–4) and an autoimmune disease known as Guillain–Barré syndrome (GBS) (5–7). Currently, no vaccine or anti-viral drugs are available for the ZIKV. Therefore, investigation of the molecular mechanisms underlying ZIKV replication, assembly and host–ZIKV interactions is urgently needed to facilitate the development of anti-viral therapeutics and vaccines.

The non-structural protein 3 (NS3) is an essential component of the viral replication and forms membrane-bound complexes with other viral proteins (8,9). The flavivirus NS3 protein contains a serine protease domain at its N-terminus, which requires a membrane-bound NS2B protein cofactor for its protease activities. The C-terminus of NS3 containing an NTP-dependent RNA helicase domain and it is mainly responsible for the hydrolysis of NTPs and the unwinding of the RNA (10–12). As a result, the NS3 helicase is an attractive target for anti-viral therapies.

Divalent metal cations are essential in assisting the NTP hydrolysis of helicases (13). Metal-independent NTP binding is not commonly observed for helicases. However, this binding may be a special property of flavivirus family NS3 helicases because it has been observed in studies of several viral NS3 helicases (13,14). Divalent metals play essential roles in the initiation of NTP hydrolysis, and the generated energy is used to drive RNA/DNA translocation in flavivirus family NS3 helicases (13,15–17).

Numerous previous structural studies of flaviviral NS3 helicases have focused on NTP hydrolysis, but the roles of metal ion binding in NTP hydrolysis, RNA unwinding and translocation have largely been ignored. As a result, the exact roles of metal cations in NTP binding/hydrolysis and nucleic acid structural rearrangement in flaviviral NS3 helicases remains poorly understood (18). Frick et al. have reported that the binding of free ATP or free magnesium ions to HCV helicase competes with $MgATP^{2-}$, the fuel for helicase movement, and leads to slower hydrolysis and nucleic acid unwinding. However, the molecular mechanism of helicase inhibition by free NTP is not known, and no structural data of free NTP-bound helicases are available.

*To whom correspondence should be addressed. Tel: +86 551 63600720; Fax: +86 551 63600831; Email: jint@ustc.edu.cn
Correspondence may also be addressed to Yajuan Li. Tel: +86 551 63600720; Email: lyj106@mail.ustc.edu.cn
†These authors contributed equally to this work as first authors.

The apo structure of ZIKV NS3 helicase at 1.80 and 1.62 Å resolution has been reported recently (19,20). In addition, the complex structures of ZIKV helicase–$MnATP^{2-}$ and ZIKV helicase–RNA reported by Tian *et al.* (21) has made the mechanism of substrate recognition much clear. However, essential roles of divalent cations in the modulation of NTP binding and hydrolysis in the flavivirus family helicases remain unclear. In this study, we determined high-resolution crystal structures of the C-terminal helicase domain of ZIKV NS3 and its complexes with nucleotides and metal ions. We obtained an NTP binding pre-activation state structure, in which only a GTPγS was bound in the NTP-binding pocket. Both the NTP-binding site and the NTP ligand undergo substantial conformational changes compared with the activation transition state observed in the complex structures containing MgGTPγS, $MnATP^{2-}$ and $MnADP^{-}$. From these results, we identified the allosteric regulatory roles of divalent metals in promoting NTP binding and local structural rearrangement, which may be applicable to other flaviviral NS3 helicases.

MATERIALS AND METHODS

Cloning, expression and purification

The coding region of NS3 gene of a ZIKV strain isolated in Guangzhou 2016 (gb: AMR39831) was synthesized by General Biosystem (Chuzhou, China). Its NS3 helicase region was amplified by PCR and ligated into a MBP tagged expression vector in a pET30a backbone. Transformed Codon Plus RIPL cells (Stratagen) were grown at 37°C until OD600 reached 1.2. Cells were then induced with 0.2 mM Isopropyl β-D-1-thiogalactopyranoside (IPTG) at 18°C for 4 h. Cells were harvested and resuspended in Ni-binding buffer (250 mM NaCl, 10 mM Imidazole, 20 mM Tris–HCl pH 8.0) supplemented with DNase (Biomatik, Canada) and protease inhibitors (Roche, USA). After sonication, soluble protein was purified from cell lysate by a HiTrap IMAC column (GE healthcare, USA), followed by a TEV protease cleavage to remove the MBP tag. The tag free helicase was obtained by a second step Ni-NTA purification followed by a Superdex-200 (GE healthcare, USA) gel filtration purification. The final protein sample resulted as a single band as revealed by SDS-PAGE.

Crystallization, data collection and structure determination

The ZIKV NS3 helicase protein was concentrated to over 100 mg/ml and high quality crystals were obtained with a condition containing 10% PEG6000, 5% MPD, 0.1M HEPES 7.5. 20% PEG200 in addition to the crystallization condition was used as the cryo-protective solution to flash-cool the crystals in liquid nitrogen. X-ray diffraction data were collected at the SSRF beamline BL-17U1, BL18U and BL-19U1. A typical data set of 360 images were collected at 12.662 keV with 1° rotation and 1 s exposure time. Data were processed with xds (22), and the space group was determined to be $P2_1$. The structure was determined by molecular replacement calculation with phaser (23) using the DENV helicase structure (PDB: 2WZQ (24)) as a searching template. The structural model was improved by rounds of manual model fitting in coot and structural optimization in phenix.refinein Phenix GUI (25). The final structural models were validated by the Molprobity server (26) and RCSB ADIT validation server (27). Molecular graphics were displayed with Pymol (Delano Scientific LLC, San Carlos, CA, USA). Protein sequence alignment was prepared with ClustalW (28). Structure superposition was done in pymol.

Differential scanning fluorimetry assay

The differential scanning fluorimetry assay was performed as reported (29). Briefly, a SYPRO orange dye in a thermal shift stability assay kit (Jason Biotech, China) was used to probe protein thermal denaturation following manufacturer's instructions. Four micromoles of ZIKV helicase protein, 100 μM nucleotides (NDPs or NTPs), 5 mM $MgCl_2$ and 100 μM sodium vanadom were mixed according to the design. 20 μl of each samples were heated using a linear gradient of 23–92°C in 20 min. Fluorescence signal as a function of temperature was recorded using a real-time PCR cycler (Bio-Rad IQ2, USA) with the excitation and emission wavelengths of 454 and 520 nm, respectively. Each sample was measured in triplet and fitted with the Boltzmann equation using GraphPad Prism (GraphPad Software, San Diego, CA, USA).

ATPase/GTPase activity assay

The ATP activity assay was carried out using the QuantiChrom™ ATPase/GTPase Assay Kit (BioAssay Systems, Hayward, CA, USA) by following product instructions. The ZIKV NS3 helicase was preincubated at a concentration of 40 nM in 20 μl assay buffer (40 mM Tris, 80 mM NaCl, 8 mM $Mg(AcO)_2$, 1 mM EDTA, pH 7.5 or 40 mM Tris, 80 mM NaCl, 1 mM EDTA, pH 7.5) in a 96-well plate. The reaction was carried out with ATP or GTP at a concentration of 0.5 mM for various time at room temperature and then terminated by adding 200 μl of reagent buffer. Followed by incubation with reagent buffer at the room temperature, the absorbance was measured at 630 nm.

RESULTS

Protein expression, crystallization and structure determination

The recombinant ZIKV NS3 helicase domain was expressed in *Escherichia coli* and purified to high homogeneity (Supplementary Figure S1). According to the results of size-exclusion chromatography, the protein existed as a monomer in solution (Supplementary Figure S1D). The apo crystals diffracted to 1.4 Å resolution, the highest resolution among the flavivirus family helicase structures solved to date. Complex structures were obtained by soaking the following substrates in the apo crystals: GTPγS, MgGTPγS, $MnATP^{2-}$ and $MnATP^{2-}$+VO_4. The ZIKV helicase structures were solved by molecular replacement by using the helicase structure of DENV (30) (Protein Databank [PDB] code: 2JLS) as a search model.

Apo structure

The ZIKV NS3 helicase/NTPase region exhibits a trilobed structure, which is a typical feature of flavivirus family mem-

bers. It is composed of three domains with approximately equal sizes, and clear clefts are located between the adjacent domains (Figure 1A and B). The apo structure was refined to 1.4 Å and yielded a final Rwork of 17.8% and Rfree of 21.3% (Table 1). The final model contained 439 residues. The Walker A motif was partially disordered, and the V248-G254 region could not be located in the electron density map.

Structural comparison

The sequence identities between the ZIKV NS3 helicase domain and those from yellow fever virus (YFV), JEV and DENV were 51%, 66% and 72%, respectively (Supplementary Figure S3). The superposition of the ZIKA helicase apo structure with other flavivirus family structures yielded RMSD values of 0.52 Å (2JLS, DENV), 1.14 Å (2WV9, Murray Valley encephalitis virus [MVEV]), 1.38 Å (2Z83, JEV) and 1.82 Å (1YKS, YFV) (Figure 1C). We noticed that the apo structure is most closely related to the ADP-complexed form of DENV helicase, whereas it is slightly different (RMSD of 1.80 Å) from the DENV helicase in complex with single-stranded RNA and ADP-VO_4 (PDB: 2JLX), which correspond to the nucleotide- and RNA ligand-bound states, respectively.

NTP-binding pocket

The ATP binding pocket is formed between domains 1 and 2. Domain 1 contains two ATP-binding motifs in the P-loop Walker A (motif I; GAGKT) and Walker B (motif II; DEAH), which are conserved among other helicase superfamilies. Domain 2 contains motif VI. In the apo structure, the Walker A motif is partially disordered, thus suggesting that it is highly flexible and may represent a resting state conformation in the absence of either a nucleotide or a RNA ligand, similarly to other helicases (30).

Metal-activated state structures

In addition to the apo structure, we obtained three metal-activated state structures in complex with $MnADP^{-}$, $MnATP^{2-}$ and MgGTPγS. The ZIKV NS3 helicase protein appeared to be active within the crystalline state, and 5 minutes of quick soaking in ATP and Mn^{2+} before flash cooling in liquid nitrogen led to the appearance of an $MnADP^{-}$ complex in the electron density map because of ATP hydrolysis. In addition, there is no clear electron density present for the free phosphate product near the β phosphate and Mn^{2+} ions, thus suggesting that the free phosphate ion vacated the pocket (30). We refined the post-hydrolysis complex structure with $MnADP^{-}$ at 1.6 Å resolution. This structure was essentially unchanged except for the NTP-binding pocket and yielded a RMSD of 0.33 Å compared with the apo structure (Figure 2D). In this structure, the Walker A motif is highly ordered and forms an extra turn at the N-terminal end of helix α1, which interacts extensively with the αβ phosphate ions (Figure 2A and B). The Mn^{2+} ion is coordinated with the β phosphate of ADP, T201 of the Walker A motif, E286 of the Walker B motif and three waters. The arginine fingers at motif VI are composed of R459 and R462, which are thought to be critical for conformational switching upon ATP hydrolysis. These fingers protrude into the nucleotide-binding pocket, and only the R462 forms hydrogen bonds with the β phosphate in the $MnADP^{-}$ complex structure.

To obtain the pre-hydrolysis complex with an intact ATP bound in the pocket, we soaked $MnATP^{2-}$+VO_4 into the helicase crystal. The electron density calculated at 1.70 Å resolution revealed the presence of an intact ATP in complex with Mn^{2+} (Figure 2C). No extra density corresponding to the VO_4 ion was apparent in the electron density map. The Mn^{2+} is coordinated with the β and γ phosphates, T201 of the Walker A motif and E286 of the Walker B motif. The attacking water (HOH8) is labeled as W-a in Figure 2C and is activated through proton transfer to E286, which functions as a base. The structure is stabilized by hydrogen bonding with the OE1 of E286, N of A317 and NE2 of Q455 in this pre-hydrolysis transition state.

Structural comparison of the pre-hydrolysis (ATP-bound) and post-hydrolysis (ADP-bound) structures in the presence of manganese ions revealed near identical structures except for the active sites (Figure 2D). The αβ phosphates and manganese ions are in identical positions in both structures, whereas the adenine bases adopt different conformations (Figure 2E). The nucleotide bases have higher B-factors and weaker electron densities than do the other tightly bound di- or tri-phosphate groups, a result that may be explained by the few nucleoside–protein interactions (discussed below).

MgGTPγS complex structure

We determined the MgGTPγS complex structure at 1.85 Å resolution (Figure 3A). The position of the GTPγS substrate superimposed well with that of ADP or ATP in the structures described above for the metal-activated states. The Mg^{2+} ion replaces the Mn^{2+} ion in the $MnATP^{2-}$ complex structure. The configuration of the nucleotide-binding pocket (Figure 3A and B), in which the GTPγS adopts an extended conformation and exhibits extensive interactions with the Walker A motif, is also highly conserved. The active water molecule is in the same position as observed in the $MnATP^{2-}$ complex.

In summary, the three tertiary complexes of ATP, ADP and GTPγS in coordination with a divalent metal either a magnesium ion or a manganese ion exhibit highly conserved structures in both the nucleotide and the nucleotide-binding pocket (Figure 2E). In addition, the overall configuration of the NTP-binding pocket and the nucleotide-metal coordinations are highly similar in the available nucleotide-metal tertiary structures of helicases from the flavivirus family and beyond (16,30). In other words, the helicase does not undergo substantial conformational changes during NTP hydrolysis, in which the γ phosphate is cleaved by a nucleophilic attack initiated by an active water stabilized by the Walker B motif and motif VI.

The GTPγS-bound structure free of metal ions represents a pre-activated state

Unexpectedly, the 1.75 Å GTPγS-bound structure free of metal ions revealed striking structural features for both the

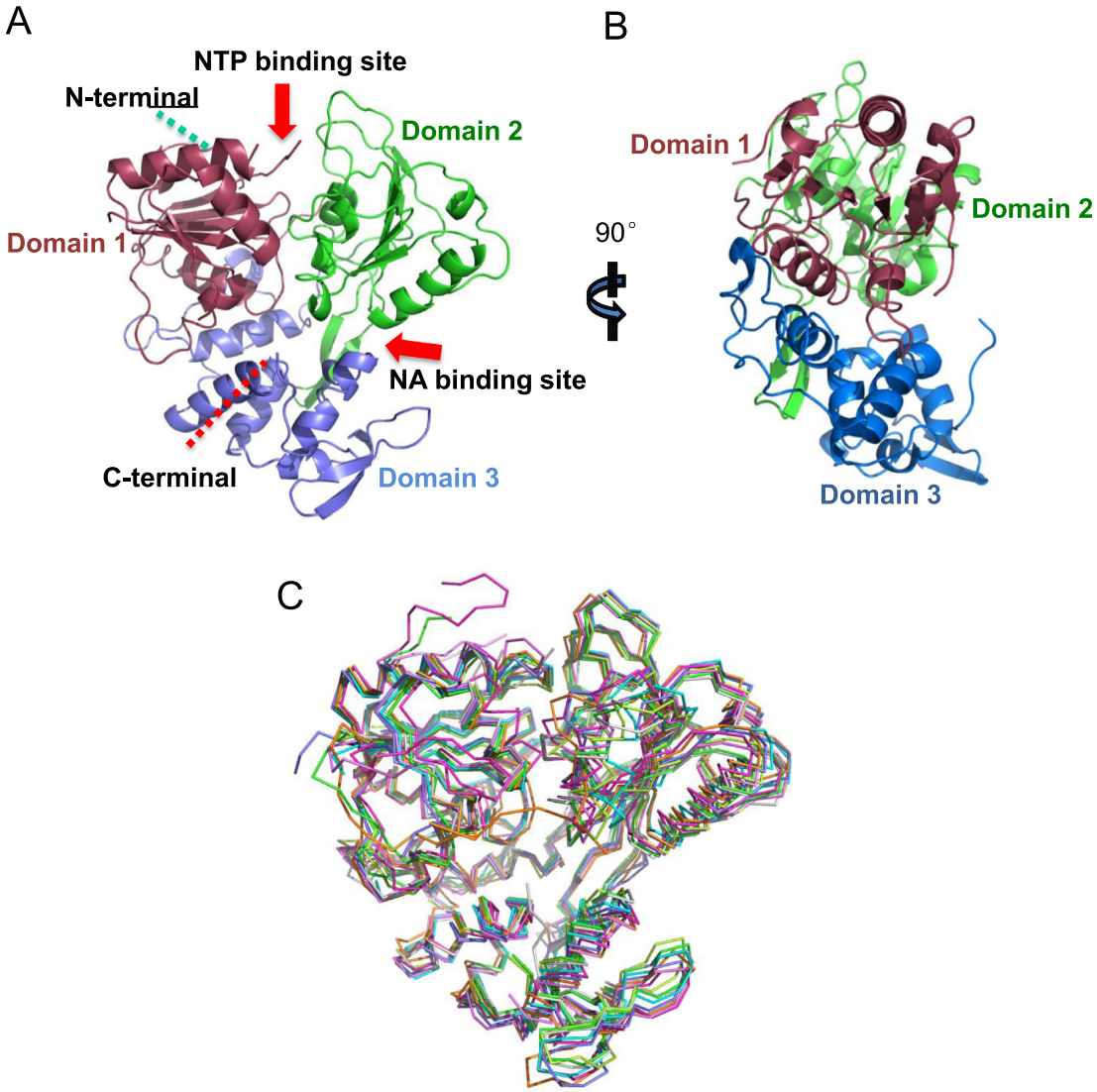

Figure 1. Overall structure of the ZIKV NS3 helicase domain. (**A**) Ribbon diagram of the apo structure showing three well-separated domains. Domains 1–3 are shown in raspberry, green and marine blue respectively. Its termini, the NTP-binding site and the NA-binding site are labeled. (**B**) Side view of the apo structure. (**C**) Structural comparison of flavivirus family viral NS3 helicases. The ZIKV apo structure is in gray. Helicases from JEV (2Z83), MVEV (2WV9), Kunjin virus (2QEQ), YFV (1YKS) and Kokobera virus (2V6I) are cyan, violet, slate, orange and lime, respectively.

nucleotide-binding pocket and the GTPγS nucleotide itself (Figure 3C–E). Detailed examination revealed that the Walker A motif interacts minimally with the triphosphate ions and that the Walker B motif does not have close contact with the GTPγS ligand. R462 in the arginine fingers forms two hydrogen bonds with the phosphates and one hydrogen bond with the ribose. The GTPγS adopts a compact conformation that decreases its interaction interface with the nucleotide-binding channel formed by the Walker A and Walker B motifs and motif VI. An internal hydrogen bond is formed between an oxygen atom of the γ-phosphate group and the hydroxyl group of the ribose (Figure 3C); this is the prominent feature of the compact ATP conformation, which is often involved in the allosteric modulation of the transduction of numerous cellular signaling pathways (31).

In the GTPγS-bound structure of NS3 helicase, there are a total of 10 hydrogen bonds between the protein and the triphosphate group, whereas 13 and 18 hydrogen bonds between nucleotide and the protein are present in the NS3-MnADP^{-} complex structure and the NS3h-MgGTPγS complex structure, respectively. This finding suggested that the compact conformation of triphosphate nucleotides results in fewer interactions with the helicase without the participation of a divalent metal ion.

Most strikingly, the Walker A motif undergoes substantial conformational changes from a GTPγS bound state to an MgGTPγS bound state. Indeed, the HPGAGK region of the Walker A motif moves as much as 5.5 Å toward the ligand (Figure 3F). However, whether this metal-induced movement of the P-loop is coupled to single-stranded RNA/DNA translocation in solution warrants further investigation.

By overlaying the two GTPγS complex structures (with and without Mg^{2+}) with the apo structure, we found that

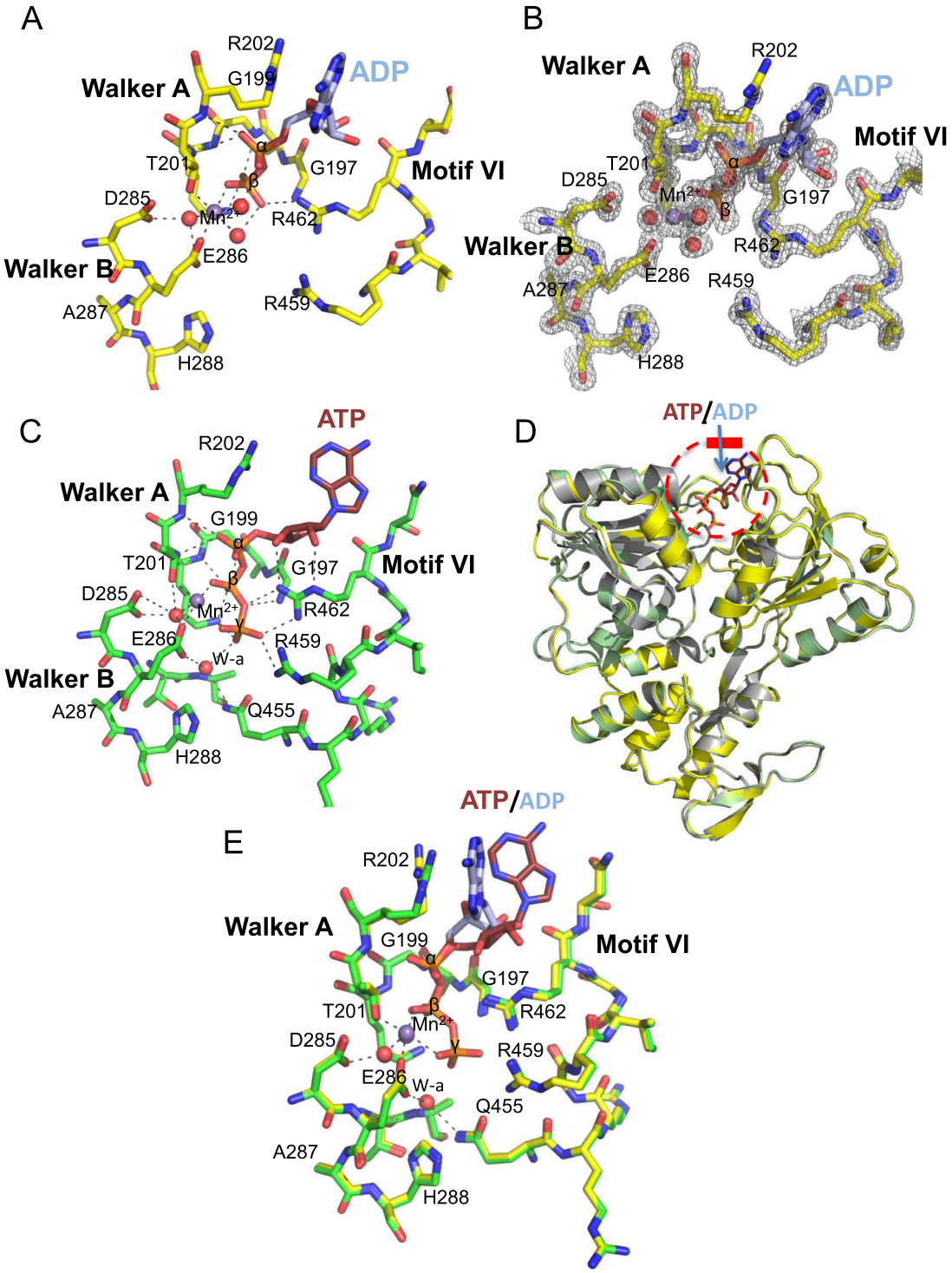

Figure 2. Nucleotide-metal tertiary complexes. (**A**) Post-hydrolysis configuration of the NTP-binding pocket bound with $MnADP^{-}$. The pocket is formed by the Walker A and Walker B motifs and motif VI. A manganese ion (shown as a purple sphere) is coordinated with β phosphate, T201 of Walker A, E286 of Walker B, and three waters. (**B**) $2F_o$ - F_c electron density map of $MnADP^{-}$ ligand calculated at 2σ. (**C**) Pre-hydrolysis configuration of the NTP-binding pocket bound with $MnATP^{2-}$. The Walker A motif, Walker B motif and motif VI are shown as green sticks. A manganese ion (shown as a purple sphere) is coordinated with βγ phosphate, T201 of Walker A, E286 of Walker B, and two waters. (**D**) Structure superposition of apo (gray), $MnATP^{2-}$ (pale green) and $MnADP^{-}$ (yellow) complexes. The NTP-binding pocket bound with an ATP molecule is circled. ATP is colored ruby. (**E**) Comparison of the $MnADP^{-}$ and $MnATP^{2-}$ complexes. The αβ phosphates and Mn^{2+} from both structures are in approximately identical positions. Only the hydrogen bonds around the Mn^{2+} and the attacking water are shown.

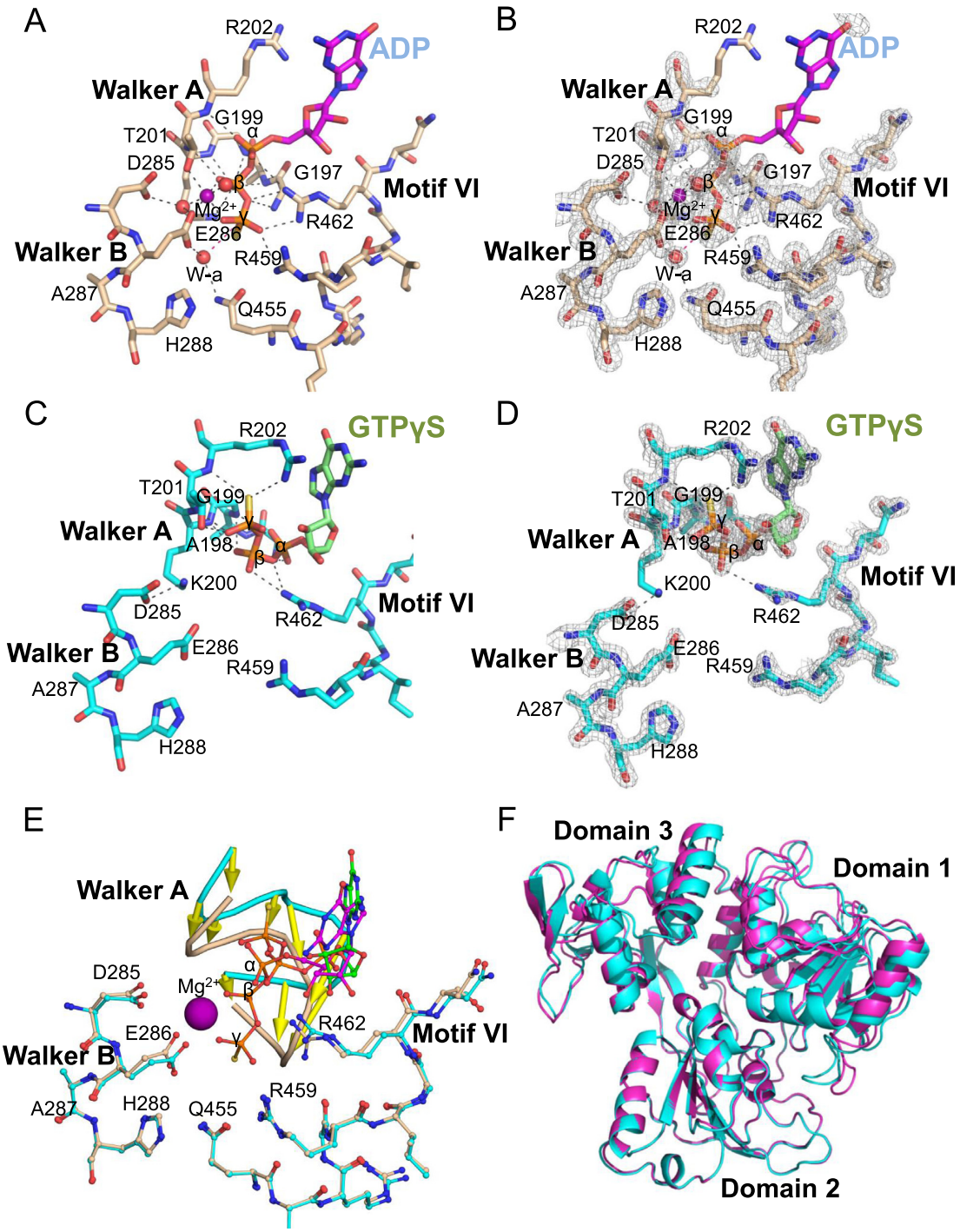

Figure 3. Activation of the NS3 helicase by divalent metals. (**A**) Pre-hydrolysis configuration of the NTP-binding pocket bound with MgGTPγS. The nucleotide-binding pocket is presented as light-orange sticks. (**B**) $2F_o$ - F_c electron density map of the MgGTPγS bound pocket calculated at 1.5σ. (**C**) NTP-binding pocket bound with free GTPγS (colored in cyan). (**D**) $2F_o$ - F_c electron density map of free GTPγS-bound pocket calculated at 2σ. (**E**) Structural comparison of the GTPγS-bound (magenta) and MgGTPγS-bound (cyan) complexes, aligned through domain 2. (**F**) Structural comparison reveals magnesium-induced conformational changes of the Walker A motif. The conformational changes of Walker A motif is indicated by arrows prepared by modevector in pymol.

Table 1. X-ray data collection and refinement table

	Apo	GTPγS	MgGTPγS	$MnATP^{2-}$ (VO_4)	$MnADP^{-}$
Spacegroup	$P12_11$	$P12_11$	$P12_11$	$P12_11$	$P12_11$
Unit cell (a, b, c) (Å)	63.29, 52.60, 65.11	64.86, 51.75, 66.2	63.95, 53.42, 65.39	63.51, 53.17, 65.11	63.49, 53.22, 64.95
(α, β, γ) (°)	90, 105.09, 90	90, 105.76, 90	90, 105.04, 90	90, 105.30, 90	90, 105.31, 90
Resolution (Å) *	50–1.40 (1.49–1.40)	50–1.75 (1.86–1.75)	50–1.85 (1.96–1.85)	50–1.70 (1.80–1.70)	50–1.60 (1.70–1.60)
No. of reflections (total/unique)	561 722/80 476	253 919/42 472	84363/34574	260905/87331	282484/53376
Redundancy*	6.89 (6.07)	5.93 (6.05)	2.44 (1.92)	2.98 (3.00)	5.29 (5.32)
Completeness (%)*	98.8 (94.8)	99.2 (99.3)	93.9 (88.2)	95.6 (92.2)	96.6 (87.5)
$I/\sigma(I)$ *	15.92 (1.81)	11.23 (1.78)	14.98 (1.59)	13.03 (1.88)	18.61(2.41)
R-meas (%)¶*	7.7 (118.3)	11.5 (113.4)	5.5 (72.2)	5.8 (71.1)	6.4 (81.7)
CC(1/2) (%)*	99.8 (67.8)	99.7 (66.6)	99.8 (65.8)	99.8 (74.6)	99.9 (80.3)
Resolution (Å)	50–1.40	50–1.75	50–1.85	50–1.70	50–1.60
Number of protein atoms	3554	3537	3482	3503	3544
No. of solvent/hetero-atoms	499	394	199	288	407
Rmsd bond lengths (Å)	0.008	0.007	0.008	0.007	0.006
Rmsd bond angles (°)	0.96	0.87	0.95	0.92	0.88
R_{work} (%)†	17.8	18.6	18.5	17.9	17.0
R_{free} (%)‡	21.3	24.0	24.7	21.6	20.0
Ramachandran plot (favored/disallowed)	98.2/0	97.5/0	97.1/0	98.0/0	98.0/0
PDB code	5JWH	5K8L	5K8T	5K8I	5K8U

*Asterisked numbers correspond to the last resolution shell.
¶ $R_{meas} = \Sigma_h(n/n\text{-}1)^{1/2}\ \Sigma_i\ |I_i(h) - <I(h)>|/\Sigma_h\Sigma_i I_i(h)$, where $I_i(h)$ and $<I(h)>$ are the ith and mean measurement of the intensity of reflection h.
† $R_{work} = \Sigma_h||F_{obs}\ (h)| - |F_{calc}\ (h)||/\Sigma_h|F_{obs}\ (h)|$, where $F_{obs}(h)$ and $F_{calc}(h)$ are the observed and calculated structure factors, respectively. No I/σ cutoff was applied.
‡ R_{free} is the R value obtained for a test set of reflections consisting of a randomly selected 10% subset of the data set excluded from refinement.
** Values from Molprobity server (http://molprobity.biochem.duke.edu/).

the NS3h–MgGTPγS complex structure is similar to the apo structure except for the Walker A motif (Supplementary Figure S2A), but is distinct to the NS3h-GTPγS complex structure (Figure 3E). The domain motion of ZIKV NS3h after Mg^{2+} binding is minor compared to $MnADP^{-}$-BeF_3 induced HCV NS3h domain 1 and domain 3 motion in the presence of ssRNA ligand (Supplementary Figure S2B). Crystallographic studies of close related DENV NS3h structures suggested that RNA binding was the major determinants that dictated the conformation of the helicase. Instead, nucleotide binding did not induce significant quaternary structural changes of DENV NS3 helicase (30).

Nucleoside-protein interaction and nucleotide preference

In our ZIKV NS3h nucleotide complex structures, both the guanosine of GTP and the adenosine of ADP/ATP are coordinated by only a guanidinium group of R202 through a cation-π interaction. Such arginine-base stacking is common in protein-nucleic acid interactions. This interaction mode suggests that the ZIKV NS3 helicase can use different types of NTPs as energy sources for RNA unwinding, as observed for the HCV NS3 helicase. Specifically, Belon and Frick have noted that all NTPs bind to the same site on the HCV helicase with similar affinities (14). Indeed, differential scanning fluorimetry assay showed that $MgNDP^{-}$s increased the thermal stability of the helicase, and different NTPs and NDPs produced close melting temperatures (T_m) among them (Figure 4A and B), suggesting that all four types of $MgNDP^{-}$s and $MgNTP^{2-}$s can bind to the ZIKV helicase. In addition, ATPase/GTPase activity assay showed that both $MgATP^{2-}$ and $MgGTP^{2-}$ were able to drive the NTPase activity of the ZIKV helicase, while such activity was dependent on Mg^{2+} ion (Figure 4C and D). This lack of discrimination among various NTP substrates may confer an evolutionary advantage for the pathogens to survive in the host. Furthermore, the absence of intensive interactions between nucleotide bases and the pocket may be the primary reason underlying the weak electron densities and high B-factors of the bases in the final refined complex structures.

DISCUSSION

Because of the lack of detailed structural information regarding the pre-activation state of the metal-free NS3 helicase in complex with NTP substrate, little is known about the molecular mechanisms underlying the metal-induced conformational changes of both NTP ligand and key residues at the Walker motifs that are involved in NTP binding. Here, we elucidated the structural basis for the metal-induced ZIKV NS3 helicase activation. Furthermore, we obtained a high-resolution structure of the metal-free GTPγS-bound complex, which resembles the pre-activation state. The GTP ligand adopts a compact conformation and has considerably fewer interactions with the nucleotide-binding pocket. In contrast, the MgGTPγS complex structure resembles an activated state configuration and exhibits a distinct extended GTP conformation with extensive interactions between $MgGTP^{2-}$ and the nucleotide-binding pocket. Structural comparison and analysis of the ZIKV NS3 helicase apo structure, pre-metal binding state structure bound with GTPγs, and metal-activated transition state structures bound with $MnADP^{-}$, $MnATP^{2-}$ and MgGTPγS revealed clear dynamic mechanisms underlying nucleotide binding, metal binding and NTPs hydrolysis. These findings provide a structural explanation for the divalent-metal-dependent conformational changes and nucleotide hydrolysis in the flavivirus NS3 helicase and probably other helicases.

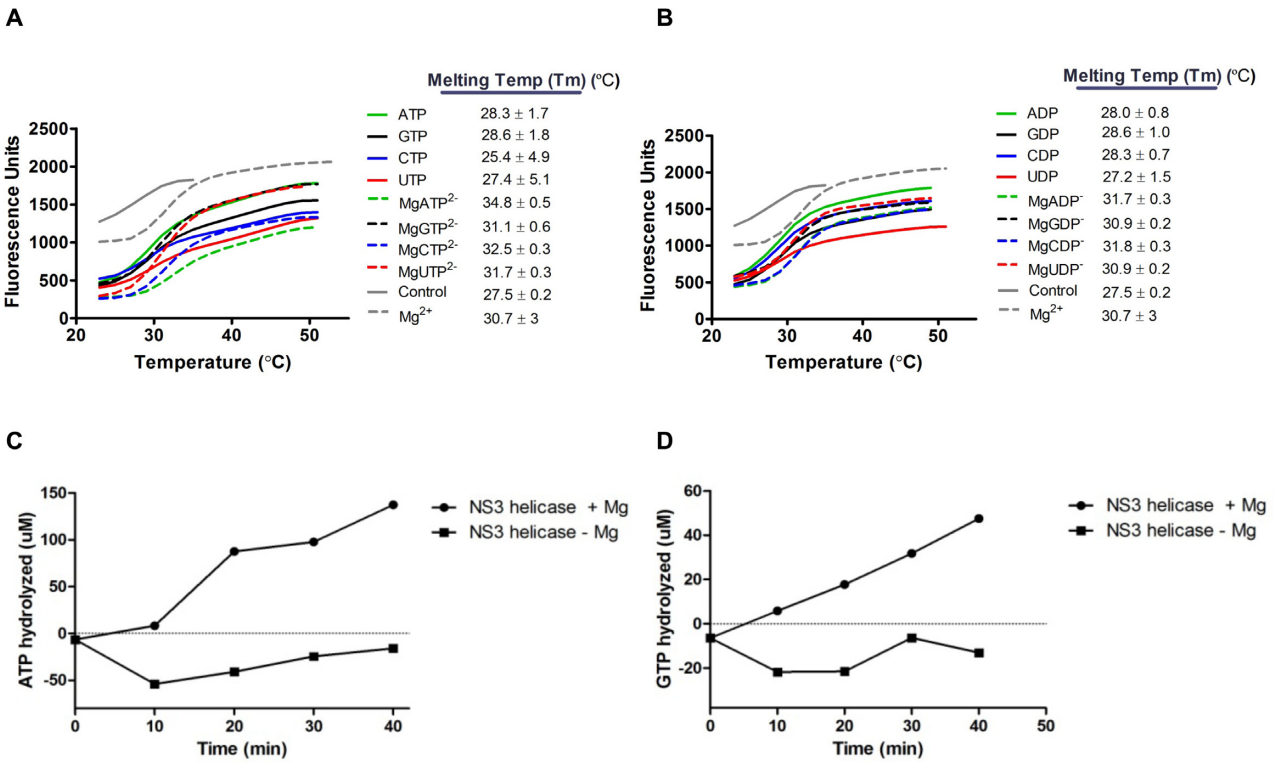

Figure 4. Nucleotide binding and hydrolysis assays. (**A**) Differential scanning fluorimetry assay shows $MgNTP^{2-}$ increases the thermal stability of ZIKV helicase. (**B**) Differential scanning fluorimetry assay shows $MgNDP^{-}$ increases the thermal stability of ZIKV helicase. (**C**) ATPase activity assay shows ATP is hydrolyzed more potently in the presence of Mg^{2+}. (**D**) GTPase activity assay shows GTP is hydrolyzed more potently in the presence of Mg^{2+}.

Two independent processes—NTP binding and NTP hydrolysis—are responsible for helicase activity

NTP molecules, such as ATP and GTP, are important allosteric modulators involved in many biological processes and also function as substrates that provide energy. Recently, two research groups have reported that its ATP-binding and ATP-hydrolysis activities play distinct roles in the activation of retinoic acid-inducible gene I (RIG-I) signaling and recycling (32,33). A mutation at the Walker A motif prevents the RIG-I receptor from binding ATP and becoming activated. In contrast, the ATPase activity of the RNA helicase RIG-I is important for the recycling of the receptor. The E373Q mutant (equivalent to the E286 of ZIKV helicase) in the Walker B motif found in some people with Singleton-Merten Syndrome, who show compromised ATPase activity, is constitutively activated by all RNA ligands, including self-RNA, thus promoting this autoimmune disease. These studies provide additional evidence that NTP binding (as an allosteric modulator) in the presence of Mg^{2+} and NTP hydrolysis (as a substrate) are two separate events and that both are important to the helicase activity. In addition, by studying the HCV NS3 helicase with optical tweezers, Dumont et al. have identified two ATP binding/hydrolysis events during the two steps of translocator movement and strand separation in a typical mechanistic cycle, thereby supporting an inchworm model (18).

Possible model of nucleic acid translocation coupled with nucleotide binding/hydrolysis

The detailed mechanism of RNA translocation coupled with NTP hydrolysis remains unclear for flavivirus family NS3 helicases. In HCV, in contrast to the Brownian motor model (34) in which the forward movement of single-stranded polynucleotides (power stroke) occurs after NTP hydrolysis when the NS3 helicase assumes the tight polynucleotide binding state along the single-stranded polynucleotide, Zhang et al. have proposed that the power stroke is triggered by NTP binding in a two-state hinge motion model (35). With two HCV NS3h-ssRNA nucleotide analog ternary complex structures, Gu and Rice were able to trap ground state and transition states, and depicted a 'ratchet' mechanism of nucleotide triggered ssRNA translocation by a SF2 helicase (36).

The present study provides new insights into the process of single-stranded polynucleotide translocation coupled with NTP binding/hydrolysis, in which the conformational changes of domain 1 and domain 2 are driven by its binding to the metal–NTP complex but not to the NTP ligand alone, as previously thought. We propose that when the helicase binds to an ssDNA, it is in a resting state as in the recently reported structure (PDB: 5GJB (21)) (Figure 5A). A free NTP can bind to the Walker A motif which results in a pre-activation state (Figure 5B). The binding of a divalent metal to the active site (E286) and the βγ phosphate of the NTP ligand drives the conformational changes of both the NTP and the Walker A motif (Figure 5C), thus resulting in

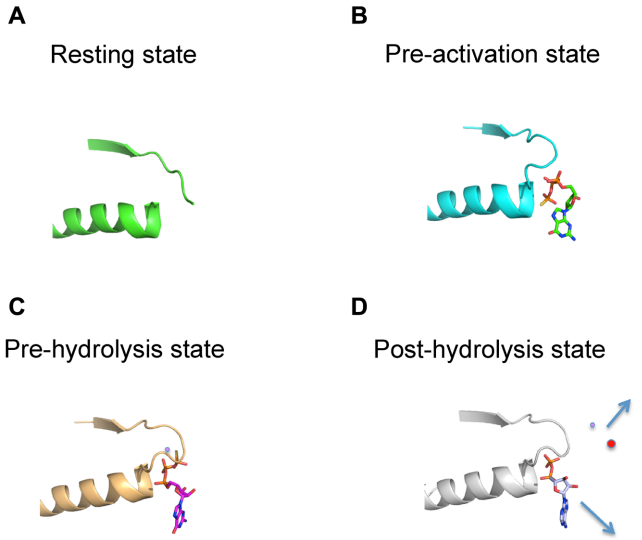

Figure 5. Snapshot of Walker A motif configuration in an NTP hydrolysis cycle. The actual structure configurations of the Walker A motif determined by our X-ray structures were presented for comparison. (**A**) In the resting state, Walker A motif may adopt multiple conformations. (**B**) In the pre-activation state, the Walker A motif binds the NTP that in compact conformation. (**C**) In the pre-hydrolysis state, the magnesium (purple sphere) binding induces the structural changes of NTP to an extended conformation. (**D**) In the post-hydrolysis state, the magnesium cation, NDP and the γ phosphate (red sphere) diffuses into the solution and the helicase returns back to the resting state.

the NTP ligand adopting an extended configuration. This configuration makes the ligand more accessible to the active water stabilized by E286 and Q455, thereby facilitating the nucleophilic attack that cleaves the γ phosphate (Figure 5D). Simultaneously, the fitting of a divalent ion and NTP into the pocket drives a conformational change of the Walker A motif; this change potentially triggers the rotation movement of domain 1 and domain 2, and is coupled with the translocation of the NA ligand. The following NTP hydrolysis step recycles the helicase, as observed for RIG-I. After the breakdown of the phosphor-anhydride linkage between the βγ phosphates, the free phosphate, metal ion and NDP readily exit the ligand-binding pocket. Because of the repulsion by domain 1, the domain 2, and the helicase returns back to the resting state with its Walker A motif return to their original conformations. The orchestra of domain movements in one NTP binding/hydrolysis cycle drives the translocation of one base of the single-stranded RNA ligand. Our results of $MgNTP^{2-}$ induced walker A conformational changes provide a useful addition to the exact mechanism of flaviviral helicase NTP dependent translocation activity.

Allosteric modulation of NS3 helicases by divalent metal cations and NTPs

In addition, we propose that the allosteric modulation of the activity of NS3 helicase by divalent metal cations and NTPs is conserved in all flaviviruses. Our structures provide a good explanation for the results of Frick *et al.* (13), in which binding of either free magnesium or free ATP to HCV helicase competes with that of $MgATP^{2-}$, the fuel for helicase movement, and leads to slower hydrolysis and nucleic acid unwinding. Our structure reveals that the compact conformation of NTP bound to the helicase is beyond the reach of the active residues, thus explaining the non-hydrolysis of NTPs in the absence of divalent metal cations (13).

Structural based design of NS3 helicase inhibitors

Development of direct-acting antiviral agents (DAAs) is in urgent needs because of the lack of effective vaccines for ZIKV. Structural and biochemical characterization of non-structural proteins as well as an in-depth understanding of the molecular basis of their activities, have contributed tremendously to the development of multiple classes of DAAs for HCV and DENV (37,38). NS3 helicase has been a challenging target to design DAAs (38). The compact conformation of NTP identified in this study provides a good starting point for the development of a potential NS3 inhibitor for the treatment of ZIKV infection.

ACCESSION NUMBERS

Coordinates and structure factors have been deposited in the Protein Data Bank, and the accession codes are presented in Table 1.

SUPPLEMENTARY DATA

Supplementary Data are available at NAR Online.

ACKNOWLEDGEMENTS

We would like to show our appreciations to Tsan 'Sam' Xiao at Case Western Reserve University, Yuzhu Zhang at Department of Agriculture, USA, and Zhengchang Liu at University of New Orleans for critical reading and comments of this manuscript. We also want to thank the staff of the BL17U1, BL18U and BL19U1 beamline at the Shanghai Synchrotron Radiation Facility (SSRF) for the assistance during data collection.
Author contributions: T.J. and Y.J.L. designed and supervised the study. X.C., Y.J.L. and X.J. conducted the experiments. X.C., Y.J.L., X.J., Y.L.L., F.G., and T.J. analyzed the data and wrote the manuscript.

FUNDING

Task Force of Zika Virus Research from the Chinese Academy of Sciences (CAS); Fundamental Research Funds for the Central Universities and the 100 Talents Program of CAS (to T.J.); China Postdoctoral Science Foundation [2015M582007 to Y.J.L.]; CAS Key Laboratory of Innate Immunity and Chronic Diseases (to F.G.). Funding for open access charge: The author.
Conflict of interest statement. None declared.

REFERENCES

1. Chen,L.H. and Hamer,D.H. (2016) Zika virus: rapid spread in the western hemisphere. *Ann. Intern. Med.*, **164**, 613–615.

2. Triunfol,M. (2016) A new mosquito-borne threat to pregnant women in Brazil. *Lancet Infect. Dis.*, **16**, 156–157.
3. Mlakar,J., Korva,M., Tul,N., Popovic,M., Poljsak-Prijatelj,M., Mraz,J., Kolenc,M., Resman Rus,K., Vesnaver Vipotnik,T., Fabjan Vodusek,V. *et al.* (2016) Zika virus associated with microcephaly. *N. Engl. J. Med.*, **374**, 951–958.
4. Li,C., Xu,D., Ye,Q., Hong,S., Jiang,Y., Liu,X., Zhang,N., Shi,L., Qin,C.F. and Xu,Z. (2016) Zika virus disrupts neural progenitor development and leads to microcephaly in mice. *Cell Stem Cell*, **19**, 120–126.
5. Roze,B., Najioullah,F., Ferge,J.L., Apetse,K., Brouste,Y., Cesaire,R., Fagour,C., Fagour,L., Hochedez,P., Jeannin,S. *et al.* (2016) Zika virus detection in urine from patients with Guillain-Barre syndrome on Martinique, January 2016. *Euro Surveill.*, **21**, doi:10.2807/1560-7917.ES.2016.21.9.30154.
6. Cao-Lormeau,V.M., Blake,A., Mons,S., Lastere,S., Roche,C., Vanhomwegen,J., Dub,T., Baudouin,L., Teissier,A., Larre,P. *et al.* (2016) Guillain-Barre Syndrome outbreak associated with Zika virus infection in French Polynesia: a case-control study. *Lancet*, **387**, 1531–1539.
7. Araujo,L.M., Ferreira,M.L. and Nascimento,O.J. (2016) Guillain-Barre syndrome associated with the Zika virus outbreak in Brazil. *Arq. Neuropsiquiatr.*, **74**, 253–255.
8. Salonen,A., Ahola,T. and Kaariainen,L. (2005) Viral RNA replication in association with cellular membranes. *Curr. Top. Microbiol. Immunol.*, **285**, 139–173.
9. Tay,M.Y., Saw,W.G., Zhao,Y., Chan,K.W., Singh,D., Chong,Y., Forwood,J.K., Ooi,E.E., Gruber,G., Lescar,J. *et al.* (2015) The C-terminal 50 amino acid residues of dengue NS3 protein are important for NS3-NS5 interaction and viral replication. *J. Biol. Chem.*, **290**, 2379–2394.
10. Matusan,A.E., Pryor,M.J., Davidson,A.D. and Wright,P.J. (2001) Mutagenesis of the Dengue virus type 2 NS3 protein within and outside helicase motifs: effects on enzyme activity and virus replication. *J. Virol.*, **75**, 9633–9643.
11. Tai,C.L., Pan,W.C., Liaw,S.H., Yang,U.C., Hwang,L.H. and Chen,D.S. (2001) Structure-based mutational analysis of the hepatitis C virus NS3 helicase. *J. Virol.*, **75**, 8289–8297.
12. Sampath,A., Xu,T., Chao,A., Luo,D., Lescar,J. and Vasudevan,S.G. (2006) Structure-based mutational analysis of the NS3 helicase from dengue virus. *J. Virol.*, **80**, 6686–6690.
13. Frick,D.N., Banik,S. and Rypma,R.S. (2007) Role of divalent metal cations in ATP hydrolysis catalyzed by the hepatitis C virus NS3 helicase: magnesium provides a bridge for ATP to fuel unwinding. *J. Mol. Biol.*, **365**, 1017–1032.
14. Belon,C.A. and Frick,D.N. (2009) Fuel specificity of the hepatitis C virus NS3 helicase. *J. Mol. Biol.*, **388**, 851–864.
15. Appleby,T.C., Anderson,R., Fedorova,O., Pyle,A.M., Wang,R., Liu,X., Brendza,K.M. and Somoza,J.R. (2011) Visualizing ATP-dependent RNA translocation by the NS3 helicase from HCV. *J. Mol. Biol.*, **405**, 1139–1153.
16. Yamashita,T., Unno,H., Mori,Y., Tani,H., Moriishi,K., Takamizawa,A., Agoh,M., Tsukihara,T. and Matsuura,Y. (2008) Crystal structure of the catalytic domain of Japanese encephalitis virus NS3 helicase/nucleoside triphosphatase at a resolution of 1.8 A. *Virology*, **373**, 426–436.
17. Benarroch,D., Selisko,B., Locatelli,G.A., Maga,G., Romette,J.L. and Canard,B. (2004) The RNA helicase, nucleotide 5′-triphosphatase, and RNA 5′-triphosphatase activities of Dengue virus protein NS3 are Mg2+-dependent and require a functional Walker B motif in the helicase catalytic core. *Virology*, **328**, 208–218.
18. Dumont,S., Cheng,W., Serebrov,V., Beran,R.K., Tinoco,I. Jr, Pyle,A.M. and Bustamante,C. (2006) RNA translocation and unwinding mechanism of HCV NS3 helicase and its coordination by ATP. *Nature*, **439**, 105–108.
19. Tian,H., Ji,X., Yang,X., Xie,W., Yang,K., Chen,C., Wu,C., Chi,H., Mu,Z., Wang,Z. *et al.* (2016) The crystal structure of Zika virus helicase: basis for antiviral drug design. *Protein Cell*, **7**, 450–454.
20. Jain,R., Coloma,J., Garcia-Sastre,A. and Aggarwal,A.K. (2016) Structure of the NS3 helicase from Zika virus. *Nat. Struct. Mol. Biol.*, **23**, 752–754.
21. Tian,H., Ji,X., Yang,X., Zhang,Z., Lu,Z., Yang,K., Chen,C., Zhao,Q., Chi,H., Mu,Z. *et al.* (2016) Structural basis of Zika virus helicase in recognizing its substrates. *Protein Cell*, **7**, 562–570.
22. Kabsch,W. (2010) Xds. *Acta Crystallogr. D Biol. Crystallogr.*, **66**, 125–132.
23. McCoy,A.J., Grosse-Kunstleve,R.W., Adams,P.D., Winn,M.D., Storoni,L.C. and Read,R.J. (2007) Phaser crystallographic software. *J. Appl. Crystallogr.*, **40**, 658–674.
24. Luo,D., Wei,N., Doan,D.N., Paradkar,P.N., Chong,Y., Davidson,A.D., Kotaka,M., Lescar,J. and Vasudevan,S.G. (2010) Flexibility between the protease and helicase domains of the dengue virus NS3 protein conferred by the linker region and its functional implications. *J. Biol. Chem.*, **285**, 18817–18827.
25. Adams,P.D., Afonine,P.V., Bunkoczi,G., Chen,V.B., Davis,I.W., Echols,N., Headd,J.J., Hung,L.W., Kapral,G.J., Grosse-Kunstleve,R.W. *et al.* (2010) PHENIX: a comprehensive Python-based system for macromolecular structure solution. *Acta Crystallogr. D Biol. Crystallogr.*, **66**, 213–221.
26. Chen,V.B., Arendall,W.B. 3rd, Headd,J.J., Keedy,D.A., Immormino,R.M., Kapral,G.J., Murray,L.W., Richardson,J.S. and Richardson,D.C. (2010) MolProbity: all-atom structure validation for macromolecular crystallography. *Acta Crystallogr. D Biol. Crystallogr.*, **66**, 12–21.
27. Yang,H., Guranovic,V., Dutta,S., Feng,Z., Berman,H.M. and Westbrook,J.D. (2004) Automated and accurate deposition of structures solved by X-ray diffraction to the Protein Data Bank. *Acta Crystallogr. D Biol. Crystallogr.*, **60**, 1833–1839.
28. Thompson,J.D., Higgins,D.G. and Gibson,T.J. (1994) CLUSTAL W: improving the sensitivity of progressive multiple sequence alignment through sequence weighting, position-specific gap penalties and weight matrix choice. *Nucleic Acids Res.*, **22**, 4673–4680.
29. Conlon,J., Burdette,D.L., Sharma,S., Bhat,N., Thompson,M., Jiang,Z., Rathinam,V.A., Monks,B., Jin,T., Xiao,T.S. *et al.* (2013) Mouse, but not human STING, binds and signals in response to the vascular disrupting agent 5,6-dimethylxanthenone-4-acetic acid. *J. Immunol.*, **190**, 5216–5225.
30. Luo,D., Xu,T., Watson,R.P., Scherer-Becker,D., Sampath,A., Jahnke,W., Yeong,S.S., Wang,C.H., Lim,S.P., Strongin,A. *et al.* (2008) Insights into RNA unwinding and ATP hydrolysis by the flavivirus NS3 protein. *EMBO J.*, **27**, 3209–3219.
31. Lu,S., Huang,W., Wang,Q., Shen,Q., Li,S., Nussinov,R. and Zhang,J. (2014) The structural basis of ATP as an allosteric modulator. *PLoS Comput. Biol.*, **10**, e1003831.
32. Rawling,D.C., Fitzgerald,M.E. and Pyle,A.M. (2015) Establishing the role of ATP for the function of the RIG-I innate immune sensor. *Elife*, **4**, e09391.
33. Lassig,C., Matheisl,S., Sparrer,K.M., de Oliveira Mann,C.C., Moldt,M., Patel,J.R., Goldeck,M., Hartmann,G., Garcia-Sastre,A., Hornung,V. *et al.* (2015) ATP hydrolysis by the viral RNA sensor RIG-I prevents unintentional recognition of self-RNA. *Elife*, **4**, e10859.
34. Levin,M.K., Gurjar,M.M. and Patel,S.S. (2003) ATP binding modulates the nucleic acid affinity of hepatitis C virus helicase. *J. Biol .Chem.*, **278**, 23311–23316.
35. Zheng,W., Liao,J.C., Brooks,B.R. and Doniach,S. (2007) Toward the mechanism of dynamical couplings and translocation in hepatitis C virus NS3 helicase using elastic network model. *Proteins*, **67**, 886–896.
36. Gu,M. and Rice,C.M. (2010) Three conformational snapshots of the hepatitis C virus NS3 helicase reveal a ratchet translocation mechanism. *Proc. Natl. Acad. Sci. U.S.A.*, **107**, 521–528.
37. Lim,S.P., Wang,Q.Y., Noble,C.G., Chen,Y.L., Dong,H., Zou,B., Yokokawa,F., Nilar,S., Smith,P., Beer,D. *et al.* (2013) Ten years of dengue drug discovery: progress and prospects. *Antiviral Res.*, **100**, 500–519.
38. Gotte,M. and Feld,J.J. (2016) Direct-acting antiviral agents for hepatitis C: structural and mechanistic insights. *Nat. Rev. Gastroenterol. Hepatol.*, **13**, 338–351.